Chapter 5

Analytical Modeling of Cogging Reduction in PM Machine

5.1 Introduction

The advent of permanent magnets with high energy density and linear demagnetization characteristic has attracted the electrical machine manufacturing industry towards development and design of high power permanent magnet (PM) machines. High power density, efficiency, power factor, torque capacity and ease of PM machines control make them advantageous over other alternative. Nowadays, the PM machine drives application widely employed in small as well as medium power applications ranging from domestic appliances for example, brushless dc (BLDC) motor for fan, blower, dryer, grinders applications and many more to medium power utilizations such as electrical vehicle drives, wind power and tidal wave energy generator. However, the cogging torque is produced in PM machine due to airgap magnetic energy variation with machine peripheral distance. Cogging torque is always a well known problem of permanent magnet machine, which may cause mechanical vibration, acoustic noise, and torque ripple. Though cogging torque is not severe problem in high speed drives as machine inertia dampen out it. However, it significantly affects the machine performance and is severe in case of light load, low speed and direct drive applications.

The interaction of permanent magnet flux and the permeance variation because of slots and tooth results in airgap magnetic energy variation with relative angular position of magnets and stator. This angular variation of airgap magnetic energy results in magnetic

torque commonly known as cogging torque and is present even in absence of armature excitation. Numerous design modifications and techniques are suggested in literatures. All these have been broadly classified as either modification of stator slots, or rotor side modification [191]. Stator side modifications include slots shifting [192], slot skewing [193], [194], teeth paring [166]and teeth notching [167], [195], auxiliary tooth [194], auxiliary slots [194], [195], tooth shape variation and slot opening variation [194]. While rotor side modifications involve magnet skewing [194], magnet shifting [192], [196], optimizing magnet pole arc to pole pitch ratio [196], [197] and machine made of different magnet pole arc [195]. Though significant cogging torque reduction is achieved by modifying both sides as slot and pole number combination [194] and optimal choice of the width ratio of armature teeth to magnet pole arc [198], but these modifications enhance design complications, and manufacturing cost. Furthermore, airgap magnetic field density get modified, which adversely reduces the magnetic flux linkage, back EMF, induced voltage and average torque of the machine.

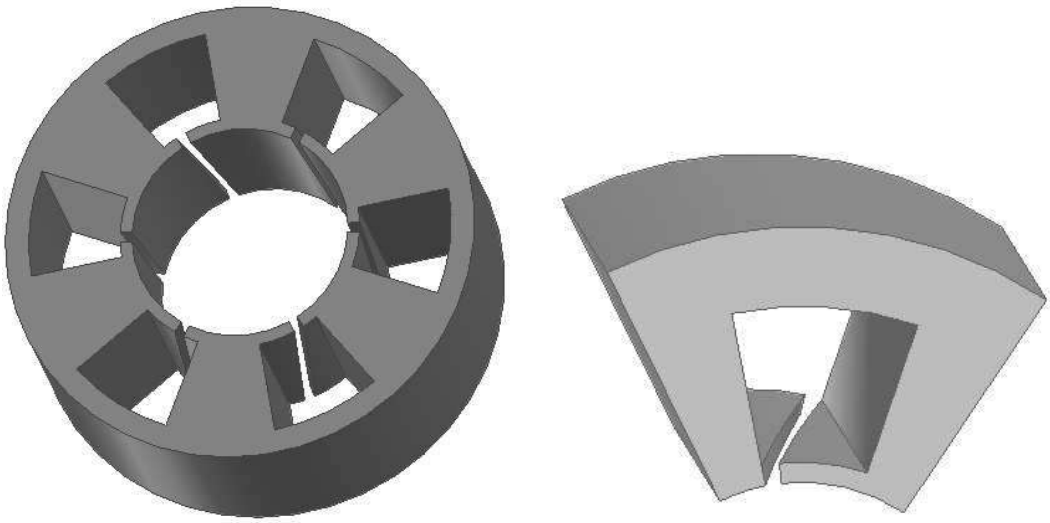

(a) Stator with Skewed Slot Opening (b) Single Slot Diagram

Figure 5.1: Permanent Magnet Machine with Skewed Slot Openings

This chapter introduces new method of cogging torque reduction in radial flux permanent magnet machines. The advantage of this method is that it does not adversely effect the machine performance. The method reduces cogging torque by skewing the slot over the slot angle. The machine topology with skewed slot opening is described in the Figure-5.1. Because of skewed slot opening, the slotting effects on the airgap flux density

displaces in peripheral while tracing along the axial direction, which results in cogging torque reduction. However, this modification does not alter the magnetic location of the slot, and hence machine performance does not get influenced significantly. In order to obtain machine performance, the field distribution in proposed machine is determined by combined methods of two dimensional subdomain analytical analysis and mutlislice method. The machine is divided into several slices and the field analysis is obtained using subdomain analysis. Hence, the field distribution in proposed machine is obtained using the superposition of solution of magnetic field for each slice. The analytical analysis developed is compared with Finite Element Analysis (FEA). The close agreement of analytical results with FEA results confirms the validation of analytical solution. Furthermore, the machine parameters viz. cogging torque, back EMF, and induced voltage are evaluated analytically, and results are compared with FEA solution. For demonstrating the effect of skewed slot opening on machine's performance, a machine of same rating without skewing the slot opening is investigated and their performances have been compared.

5.2 Analytical Modeling of Permanent Magnet Machine with Skewed Slot Opening

For the development of analytical model, the proposed machine is considered as a axial stack of stator laminated core with gradual variation of slot openings along the axial direction. The slot opening at one end of machine is at beginning of the slot, while for other end of machine, the opening is at the another end of the same slot. The angular variation of slot opening is $\alpha_{sk} = \beta_o - \alpha_o$, where α_o, and β_o are angular slot opening, and slot width.

5.2.1 No Load Magnetic Field Distributions in PM Machine

The analytical model is developed by combined use of multi-slices method, and two dimensional subdomain analysis. Following assumptions are made to establish the analytical solution

1. Machine axial length is assumed to be infinite. The end effects are ignored.

2. The permeability of stator and rotor back iron is infinite.

3. The demagnetization characteristics of magnet are linear.

4. Magnetic coupling between adjacent slices are ignored.

The slices differ with each other in location of slot opening. Taking center slice as a reference, the actual machine is modeled by considering infinitesimally small thick slice dz located at z. The angular shift of the slot opening of the this slice caused by skewing of slot opening is $\alpha_{oi} = (z/L)\alpha_{sk}$, where L is axial length of machine. The angle α_i, and β_i are central angular position of slot opening and slots of i^{th} slot, which is shown in the Figure-5.2 with respect to the reference coordinate, and are given as

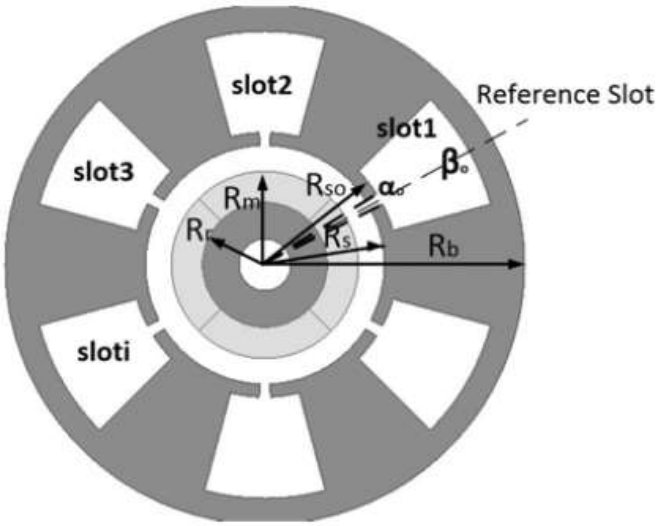

Figure 5.2: Cross Sectional View of Permanent Magnet Machine with Skewed Slot Openings

$$\begin{aligned} \alpha_i &= \tfrac{2i}{Q}\pi + \alpha_{oi} \\ \beta_i &= \tfrac{2i}{Q}\pi \end{aligned} \tag{5.1}$$

where Q is numbers of slots. The model shown in Figure-5.2 is divided into four types of regions : region 1i (i^{th} slot region), region 2i (i^{th} slot opening region), region 3 (air-gap region), and region 4 (permanent magnet region). The governing equations in coordinate frame attached with stator and centered with machine, the magnetic field $\mathbf{B}$ in terms of magnetic vector potential $\mathbf{A}$, under consideration of Coulomb's gauge $\nabla.\mathbf{A} = 0$ are given as

$$\frac{\partial^2 \mathbf{A}_{1iz}}{\partial r^2} + \frac{\partial \mathbf{A}_{1iz}}{r\partial\theta} + \frac{\partial^2 \mathbf{A}_{1iz}}{r^2\partial^2\theta} = 0 \tag{5.2}$$

$$\frac{\partial^2 \mathbf{A}_{2iz}}{\partial r^2} + \frac{\partial \mathbf{A}_{2iz}}{r\partial\theta} + \frac{\partial^2 \mathbf{A}_{2iz}}{r^2\partial^2\theta} = 0 \tag{5.3}$$

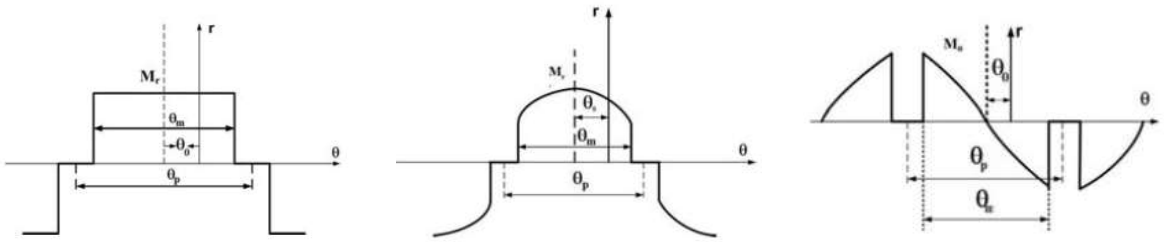

(a) (b) (c)

Figure 5.3: Magnetization Distribution of (a)Radial Component of Radial Magnetized Magnet, (b)Radial Component, and (c)Tangential Components of Parallel Magnetized Magnet

$$\frac{\partial^2 \mathbf{A}_{3z}}{\partial r^2} + \frac{\partial \mathbf{A}_{3z}}{r\partial\theta} + \frac{\partial^2 \mathbf{A}_{3z}}{r^2\partial^2\theta} = 0 \tag{5.4}$$

$$\frac{\partial^2 \mathbf{A}_{4z}}{\partial r^2} + \frac{\partial \mathbf{A}_{4z}}{r\partial\theta} + \frac{\partial^2 \mathbf{A}_{4z}}{r^2\partial^2\theta} = -\frac{\mu_o}{r}\left(M_\theta - \frac{\partial M_r}{\partial\theta}\right) \tag{5.5}$$

where, μ_o is the air permeability. M_θ, and M_r are the radial and tangential components of the residual magnetization vector, respectively. The residual magnetization of radial and parallel magnetized magnets in stator coordinate frame are shown in the Figure-5.3 [102], which are expressed in Fourier Series expansion as [199]

$$\begin{aligned} M_r &= \sum_{n=1,3,5...}^{\infty} M_{rn}\cos(n(\theta+\theta_0)) \\ M_\theta &= \sum_{n=1,3,5...}^{\infty} M_{\theta n}\sin(n(\theta-\theta_0)) \end{aligned} \tag{5.6}$$

where $\theta_0 = \omega_r t - \theta_i$, ω_r is rotor angular speed and θ_o is initial rotor position with respect to the reference slot. The M_{rn}, and $M_{\theta n}$ for radial and parallel magnetized magnet are given by equations (5.7), and (5.8), respectively.

$$M_{rn} = (4B_r p/\mu_0 n\pi) sin(n\pi\alpha_p/2p); \qquad M_{\theta n} = 0; \qquad \forall \ \tfrac{n}{p} = 1,3,5... \tag{5.7}$$

and,

$$M_{rn} = B_r\alpha_p(C_{1n}+C_{2n})/\mu_0; \qquad M_{\theta n} = B_\theta\alpha_p(C_{1n}-C_{2n})/\mu_0; \qquad \forall \ \tfrac{n}{p} = 1,3,5... \tag{5.8}$$

where, C_{1n}, and C_{2n} are given by equation (5.9).

$$C_{1n} = \frac{\sin[(np+1)\alpha_p\frac{\pi}{2p}]}{(np+1)\alpha_p\frac{\pi}{2p}}; \qquad C_{2n} = \begin{cases} 1 & \text{for np} = 1 \\ \frac{\sin[(np+1)\alpha_p\frac{\pi}{2p}]}{(np+1)\alpha_p\frac{\pi}{2p}} & \text{for np} \neq 1 \end{cases} \tag{5.9}$$

where B_r is the residual flux density of the magnet. The solutions of the governing field equations (5.2)-(5.5) are obtained using the boundary conditions as described bellow

The boundary conditions to be followed by the slot regions are

$$\mathbf{B}_{1i\theta}(r,\theta)|_{r=R_b} = 0 \tag{5.10}$$

$$\mathbf{B}_{1ir}(\theta,z) = 0; \forall\theta \in \left\{-\frac{\beta_o}{2}+\beta_i, \frac{\beta_o}{2}+\beta_i\right\} \tag{5.11}$$

In view of above boundary condition, the vector potential in slot region is periodic in peripheral direction. Applying variable separable method for solving differential equation, the solution of governing field equation. represented by the equation (5.2) is given as

$$\mathbf{A}_{1iz} = \sum_{k=1}^{\infty} a_{1in}\left(\left(\frac{R_s}{R_b}\right)^{E_k}\left(\frac{r}{R_b}\right)^{E_k} + \left(\frac{r}{R_s}\right)^{-E_k}\right) \times \cos E_k\left(\theta+\frac{\beta_o}{2}\right) \tag{5.12}$$

and, the boundary condition at the lateral edge of slot opening regions are

$$\mathbf{B}_{2ir}(\theta,z) = 0; \forall\theta \in \left\{-\frac{\alpha_i}{2}+\beta_i, \frac{\alpha_i}{2}+\beta_i\right\} \tag{5.13}$$

and, the correspondingly the solution of the governing field equation. given by the equation (5.3) is

$$\mathbf{A}_{2iz} = \sum_{m=1}^{\infty}\left(a_{2in}\left(\frac{r}{R_s}\right)^{F_m} + b_{2in}\left(\frac{r}{R_{so}}\right)^{-F_m}\right) \times \cos F_m\left(\theta+\frac{\beta_o}{2}-\alpha_{so}\right) \tag{5.14}$$

where, $E_k = k\pi/\beta_o$, and $F_m = m\pi/\alpha_o$ are harmonics order of magnetic field distributions in slot opening and slot regions, respectively.

Other boundary conditions are applied at $r = R_{so}$, $r = R_s$ and R_m. These boundary conditions ensures continuity of radial flux density, and tangential field intensity as demonstrated below:

The boundary conditions at $r = R_{so}$ are

$$\mathbf{B}_{2ir} = \mathbf{B}_{1ir}|_{r=R_{so}} \tag{5.15}$$

and,

$$\mathbf{H}_{1i\theta}|_{r=R_{so}} = \begin{cases} \mathbf{H}_{2i\theta}; \forall\theta \in \left[-\frac{\alpha_i}{2}+\beta_i, \frac{\alpha_i}{2}+\beta_i\right] \\ 0; \theta \notin \left[-\frac{\alpha_i}{2}+\beta_i, \frac{\alpha_i}{2}+\beta_i\right] \end{cases} \tag{5.16}$$

The boundary conditions at $r = R_s$ are

$$\mathbf{B}_{1ir} = \mathbf{B}_{2ir}|_{r=R_s} \tag{5.17}$$

and,

$$\mathbf{H}_{2\theta}|_{r=R_s} = \begin{cases} \mathbf{H}_{1i\theta}; \forall\theta \in \left[-\frac{\alpha_i}{2}+\beta_i, \frac{\alpha_i}{2}+\beta_i\right] \\ 0; \forall\theta \notin \left[-\frac{\alpha_i}{2}+\beta_i, \frac{\alpha_i}{2}+\beta_i\right] \end{cases} \tag{5.18}$$

The boundary conditions at $r = R_m$ are

$$\mathbf{H}_{3\theta} = \mathbf{H}_{4\theta}|_{r=R_m} \tag{5.19}$$

$$\mathbf{B}_{3r} = \mathbf{B}_{4r}|_{r=R_m} \tag{5.20}$$

The last boundary conditions is the zero tangential flux density at the rotor back iron, which is mathematically given as

$$\mathbf{B}_{4\theta}(\theta, z)|_{r=R_r} = 0 \tag{5.21}$$

Applying variable separable method, the vector potentials in rest two regions are expressed as [199]- [121]

$$\mathbf{A}_{3z} = \sum_{n=1}^{\infty}\left(a_{3n}\left(\frac{r}{R_{so}}\right)^n + b_{3n}\left(\frac{r}{R_m}\right)^{-n}\right)\cos(n\theta) + \sum_{n=1}^{\infty}\left(c_{3n}\left(\frac{r}{R_{so}}\right)^n + d_{3n}\left(\frac{r}{R_m}\right)^{-n}\right)\sin(n\theta) \tag{5.22}$$

and,

$$\mathbf{A}_{4z} = \mathbf{A}_{4p} + \sum_{n=1}^{\infty}\left(a_{4n}\left(\frac{r}{R_m}\right)^n + b_{4n}\left(\frac{r}{R_r}\right)^{-n}\right)\cos(n\theta) + \sum_{n=1}^{\infty}\left(c_{4n}\left(\frac{r}{R_m}\right)^n + d_{4n}\left(\frac{r}{R_r}\right)^{-n}\right)\sin(n\theta) \tag{5.23}$$

where $\mathbf{A}_{4p}$ is the particular solution of equation (5.5). All the coefficients involved in solutions are evaluated using aforementioned boundary conditions. The mathematical development of the linear simultaneous equations are similar to approach explained in Appendix E.

5.2.2 Cogging Torque, Flux Linkage , And Induced Voltage Calculation

Numerous analytical methods are developed to estimate the cogging torque in PM machines. Recent papers [169], [200] have summarized and compared analytical methods for cogging torque calculation in surface mounted PM machines. The authors discussed pros and cons of analytical models for predicting the cogging torque in PM machines. They incorporated four analytical models which are : based on energy variation method, lateral

force (LF), complex permeance (CP), exact subdomain (SD) models and superposition technique of cogging torque. In energy variation method, the cogging torque is calculated from airgap magnetic energy variation with the angular rotation. The assumption of no fluxes crossing slots i.e., all flux are confined to tooth regions excludes the magnetic energy variation in the tooth [167] results in cogging torque prediction discrepancy. However, the LF method is based on the assumption that the magnetic flux lines have semicircular paths in the slots and relative permeance is introduced [192]. For the calculation of cogging torque, the radial and tangential components of magnetic field are evaluated by use of magnetic field densities in slotless machine and slotting effects incorporates with relative permeance [192], [89]. This method accurately predicts radial flux density and the discrepancy in tangential component arises due to the assumption made for flux lines in slots. The complex permeance (CP) method is based on the conformal mapping which transform slotted machine into slotless machine, in order to predict airgap magnetic field density [106]. The cogging torque can be obtained by applying the Maxwell stress tensor on a circular path in the air gap. However, complexity is increased as numerical iterative solution is required for complex permeance function calculation. Moreover, the CP model assumes no shape deformations in the magnets and a circular path to predict the air-gap flux density. However, the deformations do occur when the slotted machine is mapped to the slotless machine [200]. Hence, the assumption results in errors in the predicting air-gap flux density. In exact subdomain (SD) models, the field domain is divided into three types of SDs, viz., magnets, air gaps, and slots. The expression of field distribution in each SD is derived separately. The field solution is obtained by applying the boundary and interface conditions [116], [121], [122] and [201]. However, the subdomain model takes significantly long computational time, since it requires to solve M^2 or $N_s^2M^2$sets of equations, where M is harmonics order, and N_s the number of slots. Nevertheless, the complexity is reduced by use of superposition technique [202], [203]. The supposition techniques evaluates the cogging toque produced in machine by superposition of cogging torque produced by individual slot of machine with assumption that there is no mutual influence of slots. This assumption results in magnetic field as well as cogging torque prediction error.

The exact SD model is the most accurate among all analytical model which accounts the mutual influence between slots. In view of this, the analytical model developed in

previous section is used for cogging torque calculation. The obtained radial and tangential components of airgap magnetic field density is further used for flux linkage , and induced voltage calculation. The cogging torque is calculated using Maxwell Stress tensor and for infinitesimally small length (dz) machine the cogging torque is expressed as

$$dt_{cog} = \frac{r^2 dz}{\mu_o} \int_0^{2\pi} B_{3r} B_{3\theta} d\theta \tag{5.24}$$

where, B_{3r}, and $B_{3\theta}$ are radial and tangential flux density components at PM surface. The total cogging developed in machine is calculated as integration of cogging torque produced due to elementary machine portion over its length.

$$T_{cog} = \int_{-L_a/2}^{L_a/2} \int_0^{2\pi} \frac{r^2}{\mu_o} B_{2r} B_{2\theta} d\theta dz \tag{5.25}$$

The flux linkage ϕ_i per phase is calculated as

$$\phi_i = \int_{-L_a/2}^{L_a/2} \int_i \frac{N_c R_s}{a} B_{2r} d\theta dz \tag{5.26}$$

where $i = A, B, \& C$ represents phases of the stator winding, N_c is the number of turns per phase, and a is the parallel- circuits per phase. The induced voltage per phase in the winding is evaluated by

$$E_i = -\frac{d\phi_i}{dt} \tag{5.27}$$

5.3 Comparison of Analytical and FEA Analysis

For the validation of the analytical model, a 3D FEM model of PM machine is simulated in ANSOFT MAXWELL 18.0 as shown in Figure-F.4. The developed model is enclosed within a boundary (region) and Neumann condition is assigned to the boundary. The machine dimensions given in Table 5.1 is used. The machine's slot opening is skewed with an angle 25^o. The slot opening angular position vary with axial length of machine and hence their effect on the magnetic field is different. For evaluating the effects of slot opening displacement, the radial and tangential components of magnetic field density at different axial length: $1/4^{th}$, and $1/2^{th}$, is obtained from analytical solution and compared with FEA results. These comparison are shown in the Figures-5.4 and 5.5. Furthermore,

Table 5.1: Machine Parameter for Analysis

Parameters	Variable	Value
No of poles	P	4
No of Slots	Q_s	6
Axial Length	L_a	100 mm
Rotor Radius	R_r	18 mm
Magnet Radius	R_m	22 mm
Stator Bore Radius	R_s	23 mm
Slots Inner Radius	R_s	25.5 mm
Slots Outer Radius	R_s	45 mm
Slots Opening	α_o	5^o
Slots Width	β_o	30^o
Opening Skew	θ_{ok}	25^o
Remanent Magnetization	B_r	1.1 Tesla
Relative Permeability	μ_r	1.05

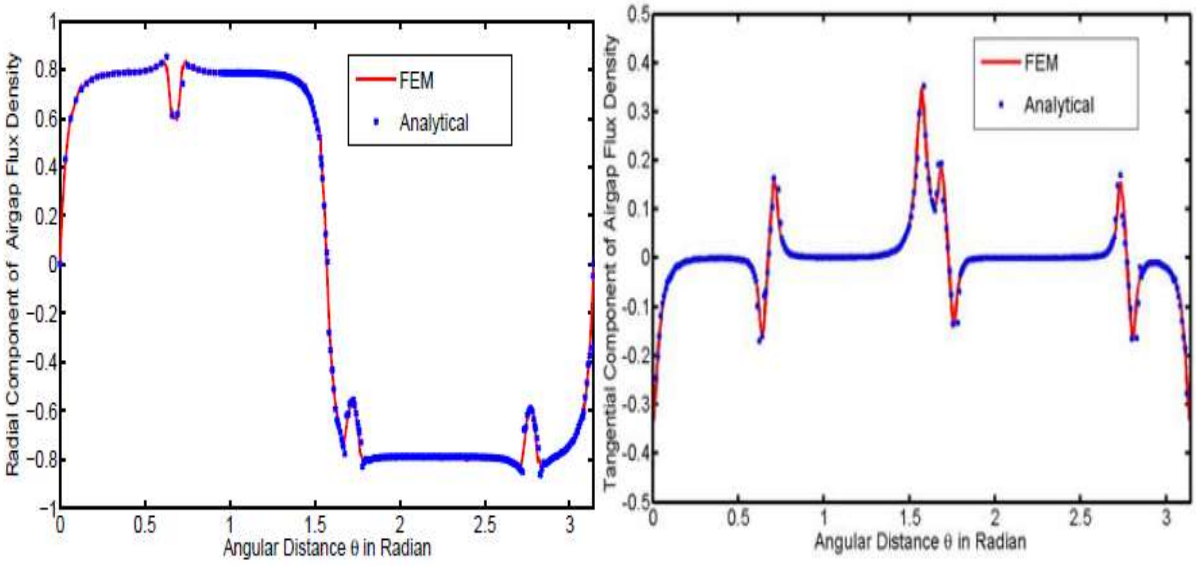

(a) (b)

Figure 5.4: Comparison of B_r, and B_t at $r = (R_m + R_s)/2$, and $Z = 25mm$

the effect of skewed slot opening is realized by plotting the magnetic field densities at different axial length as shown in the Figure-5.6. Relative location of slotting effects

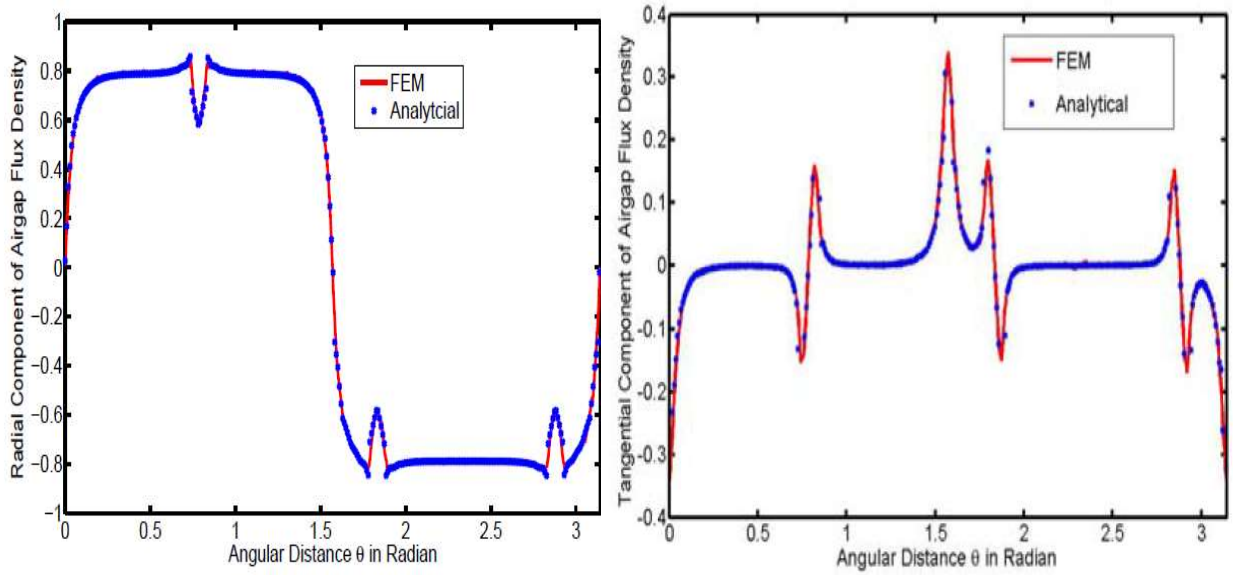

(a) (b)

Figure 5.5: Comparison of B_r, and B_t at $r = (R_m + R_s)/2$, and $Z = 50mm$

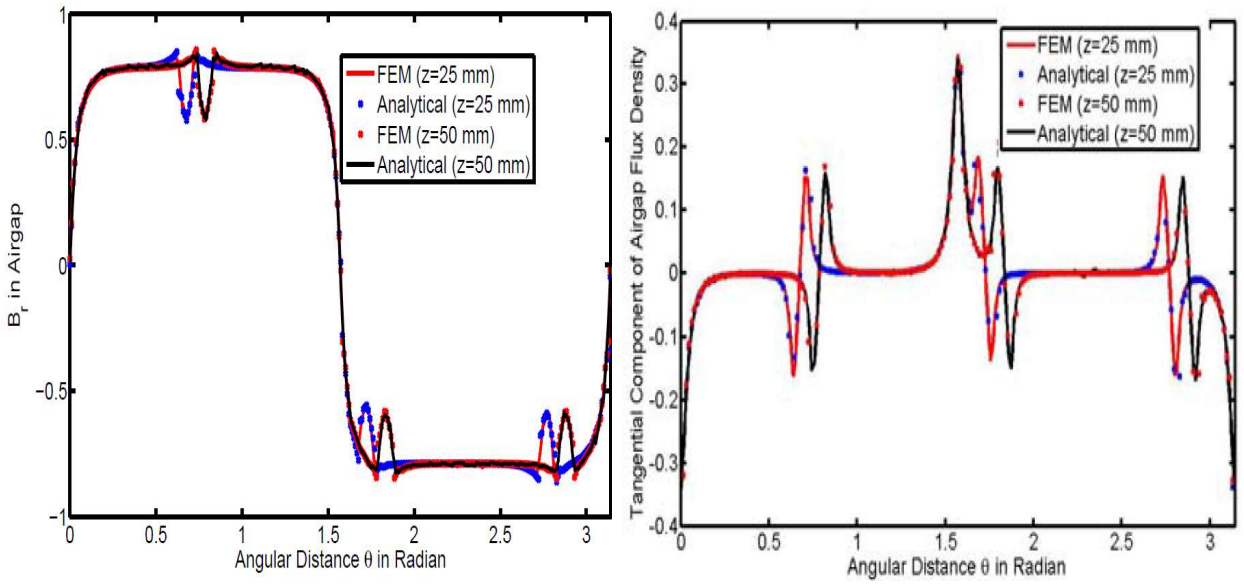

(a) (b)

Figure 5.6: Effect of Slot Opening on Radial Flux Density, and Tangential Flux Density

in the machine changes with axial position. This contributes to a phase displacement in cogging torque produced by each slice, which results in reduction of total cogging torque developed in machine. Because of the same reason the cogging torque reduces in skewed slots permanent magnet machine. However, in skewed slots machine, the magnetic position of armature coil along axial length changes and hence results in reduction of both

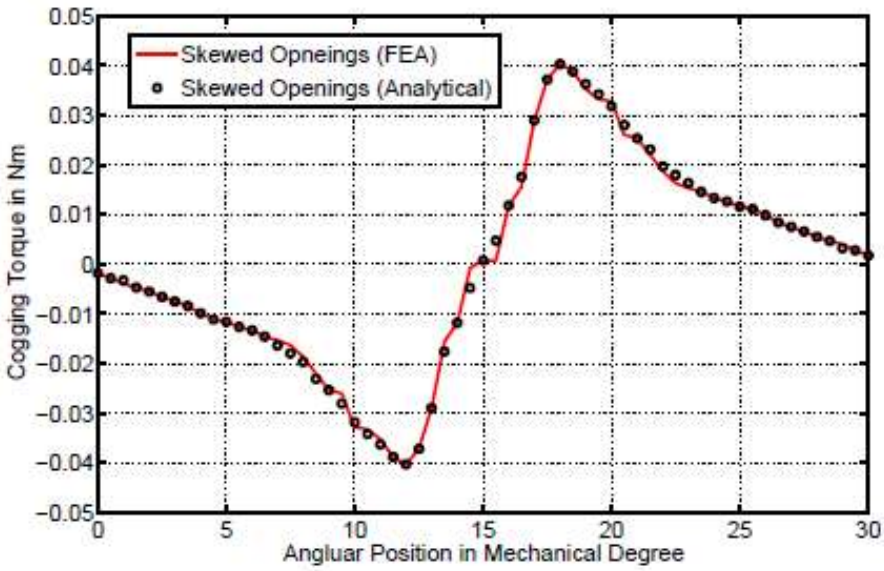

Figure 5.7: Cogging Torque in Skewed Opening Machine

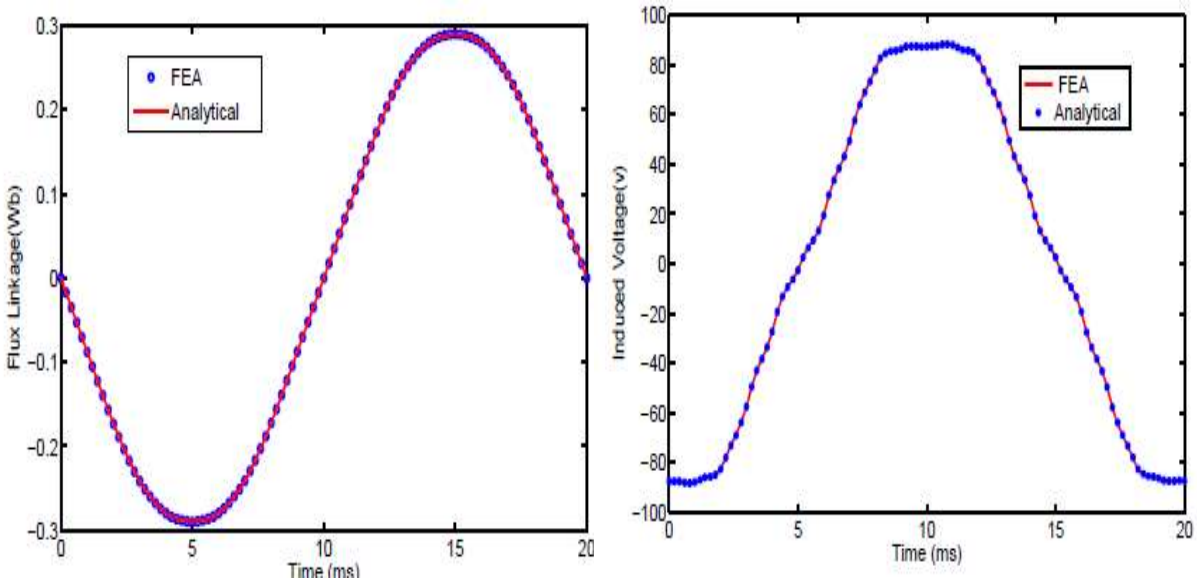

(a) Flux Linkage

(b) Induced Voltage

Figure 5.8: Comparison of Analytical and FEM Analysis

the flux linkage and induced voltage. The cogging torque, linkage flux and phase voltage in the machine is shown in the Figure-5.7 and Figure-5.8. In order to elaborate the advantages of proposed method for cogging reduction, the performance of this machine and a machine with unskewed opening is obtained. The parameters of unskewed slot opening machine are kept same as the proposed machine's parameters and given in the table 5.1 with the skewing angle θ_{ok} is zero. Further analysis and comparison of cogging

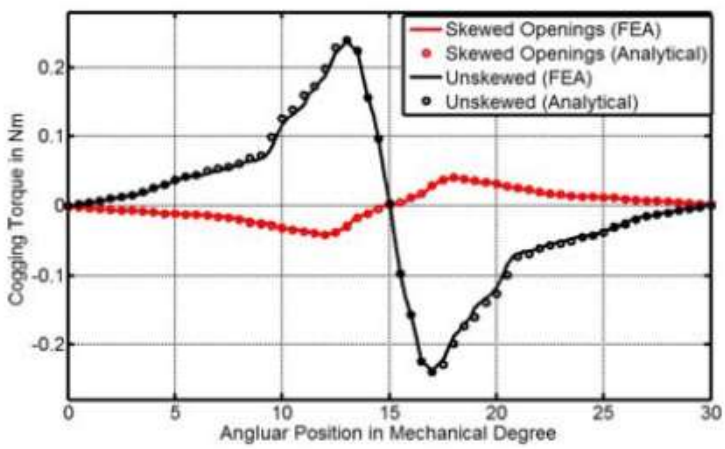

Figure 5.9: Cogging Torque Comparison

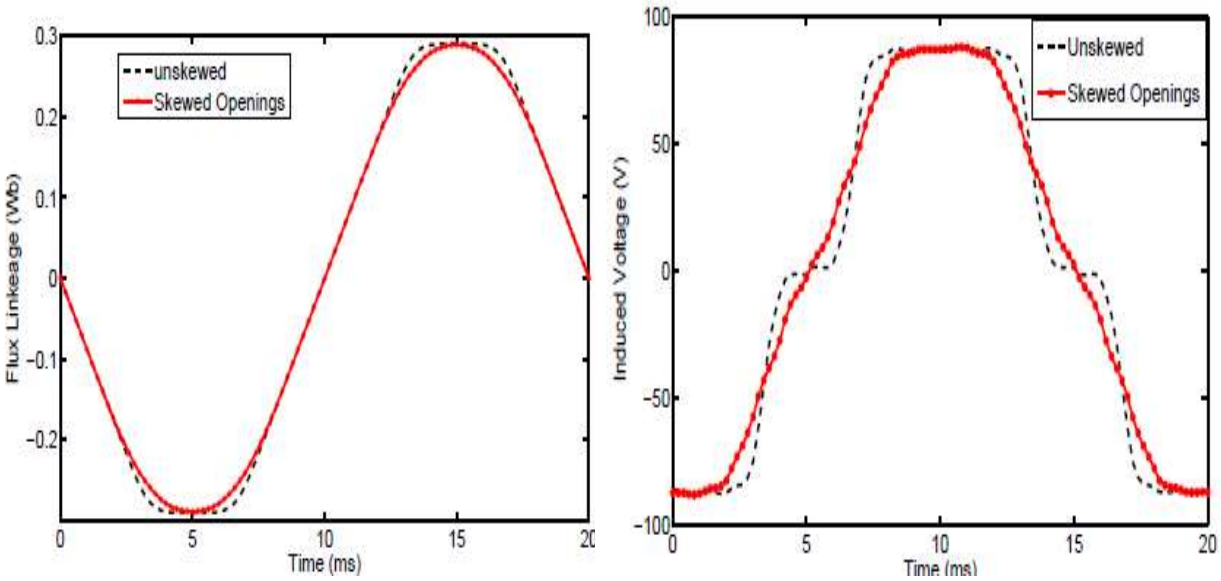

(a) Flux Linkage (b) Induced Voltage

Figure 5.10: Flux Linkage and Phase Voltage Comparison

torque, flux linkage and induced voltage are shown in Figure-5.9 and Figure-5.10. Figure-5.9 shows sufficient reduction in cogging torque, while Figure-5.10 demonstrate marginal reduction in linkage flux and phase voltage.

5.4 Conclusion

A new method for cogging torque reduction via skewed opening in PM machine is proposed. For analyzing the effect of slot opening skewing on machine performance, an

analytical model is developed. The analytical analysis is validated with FEM results. Investigation suggests 83% of cogging reduction in permanent magnet machine can be achieved by skewing the slot openings. Furthermore, the flux linkage and induced voltage reduction is insignificant for skewed openings machine. This method of cogging reduction is advantageous than reported methods as the direct axis of rotor and stator are parallel to each other throughout machine's axial length. Hence, this design modification does not increase the complexity of machine control as it happens with others methods.